In preparation for submission to *Solar Physics*
http://www.springerlink.com/content/0038-0938

Effects of Field-Aligned Flows on Standing Kink and Sausage Modes Supported by Coronal Loops

S.-X. Chen · B. Li · L.-D. Xia · Y.-J. Chen · H. Yu

Received: •••••••••••• / Accepted: •••••••••••• / Published online: ••••••••••••

Abstract Fundamental standing modes and their overtones play an important role in coronal seismology. We examine how a significant field-aligned flow affects standing modes supported by coronal loops, modeled here as cold magnetic slabs. Of particular interest are the period ratios of the fundamental to its $(n-1)^{\rm th}$ overtone (P_1/nP_n) for both kink and sausage modes, and the threshold half-width-to-length ratio for sausage modes. For standing kink modes, the flow significantly reduces P_1/nP_n in general, the effect being particularly strong for larger n and when the density contrast $\rho_0/\rho_{\rm e}$ between loops and their surroundings is weak. That said, even when $\rho_0/\rho_{\rm e}$ approaches infinity, this effect is still substantial, reducing the minimal P_1/nP_n by up to 13.7 % (24.5 %) for $n=2$ ($n=4$) relative to the static case, when the Alfvén Mach number M_A reaches 0.8 where M_A measures the loop flow speed in units of the internal Alfvén speed. For standing sausage modes, although not negligible, the flow effect in reducing P_1/nP_n is not as strong. However, the threshold half-width-to-length ratio is considerably larger in the flowing case than its static counterpart. For $\rho_0/\rho_{\rm e}$ in the range $[9, 1024]$ and M_A in the range $[0, 0.5]$, an exhaustive parameter study yields that this threshold is well fitted by our Equation (23) which involves the two parameters in a simple way. This allows one to analytically constrain the combination $(\rho_0/\rho_{\rm e}, M_A)$ for a loop with known width-to-length ratio when a standing sausage oscillation is identified therein. It also allows one to further examine the idea of partial sausage modes, and the flow is found to reduce significantly the spatial extent where partial modes are allowed.

Keywords: Coronal Seismology; Magnetic fields, Corona; Waves, Magnetohydrodynamic; Waves, Propagation.

Shandong Provincial Key Laboratory of Optical Astronomy and Solar-Terrestrial Environment, School of Space Science and Physics, Shandong University at Weihai, 264209 Weihai, China email: bbl@sdu.edu.cn

1. Introduction

Combining the measured parameters of the abundant low-frequency waves and oscillations in the solar corona with magnetohydrodynamic (MHD) wave theory, coronal seismology offers the capability for deducing the parameters of the structured corona that prove difficult to be directly found (see, *e.g.* the reviews by Roberts, 2000; Nakariakov and Verwichte, 2005; Roberts, 2008; Nakariakov and Erdélyi, 2009; Erdélyi and Goossens, 2011; De Moortel and Nakariakov, 2012). Both slow and fast waves have been found important for seismological purposes. Regarding slow waves, the observed instances appear both as standing modes (see Wang, 2011, and references therein) and in the form of propagating waves (for recent reviews, see De Moortel, 2006; Banerjee *et al.*, 2007; De Moortel, 2009). Likewise, propagating fast waves were identified in eclipse measurements of active-region loops (Williams *et al.*, 2001, 2002), and in apparently open structures as indicated by the *Transition Region and Corona Explorer* (TRACE: Handy *et al.* (1999)) measurements of a post-flare supra-arcade (Verwichte, Nakariakov, and Cooper, 2005) and the more recent *Solar Dynamics Observatory/Atmospheric Imaging Assembly* (SDO/AIA: Pesnell, Thompson, and Chamberlin (2012); Lemen *et al.* (2012)) measurements of a funnel of loops (Liu *et al.*, 2011). Moreover, standing kink oscillations in coronal loops, directly imaged by TRACE and first reported by Nakariakov *et al.* (1999) and Aschwanden *et al.* (1999), seem to abound also in loops measured by the *Hinode* experiment (*e.g.* Ofman and Wang, 2008; Erdélyi and Taroyan, 2008) (also see Kosugi *et al.*, 2007, for an overview of the instruments), *Solar TErrestrial RElations Observatories/Sun Earth Connection Coronal and Heliospheric Investigation* (STEREO/SECCHI) (*e.g.* Verwichte *et al.*, 2009) (for an instrument overview, see Kaiser *et al.*, 2008; Howard *et al.*, 2008), SDO (*e.g.* Aschwanden and Schrijver, 2011; White and Verwichte, 2012), to name but a few missions.

The multiple periods found in a number of loops experiencing standing kink oscillations, interpreted as the fundamental mode and its higher order overtones, have found extensive seismological applications (see, *e.g.*, Andries *et al.*, 2009; Ruderman and Erdélyi, 2009, for recent reviews). The observational basis is that the period ratio $[P_1/nP_n]$ tends to deviate from unity, where P_1 denotes the period of the fundamental mode, and P_n denotes that of its $(n-1)^{\rm th}$ overtone with $n = 2, 3, \ldots$ The first evidence for such a behavior was presented by Verwichte *et al.* (2004) using TRACE 171Å imaging data, where $P_1/2P_2$ was found to be 0.91 and 0.82 in the two cases examined therein, which were corroborated by a further study of the same events (Table 2 in Van Doorsselaere, Nakariakov, and Verwichte, 2007). Examining a new event also imaged by TRACE in its 171Å passband, this latter study yielded a value for $P_1/2P_2$ of 0.9. Actually, periods of even higher-order overtones were also detected both in TRACE data (Van Doorsselaere, Birtill, and Evans, 2009) (see also De Moortel and Brady 2007) and in the *Nobeyama RadioHeliograph* (NoRH) data (Kupriyanova, Melnikov, and Shibasaki, 2013). In the former study, $P_1/2P_2$ and $P_1/3P_3$ were found to be 0.99 and 0.965, respectively. In the latter, these read 0.83 and 0.91. Among the mechanisms that may contribute to the departure of P_1/nP_n from unity, for thin

EUV loops it is concluded that the density stratification (*e.g.* Andries, Arregui, and Goossens, 2005; Donnelly, Díaz, and Roberts, 2006; McEwan *et al.*, 2006) (see also the review by Andries *et al.* 2009) and lateral expansion (Verth and Erdélyi, 2008; Ruderman, Verth, and Erdélyi, 2008) along the loop play the most prominent role. The direct observational consequence is that one may deduce the longitudinal density scale height $[H_\rho]$ using $1 - P_1/2P_2$, as was first advocated by Andries, Arregui, and Goossens (2005), and may combine $1 - P_1/2P_2$ and $1 - P_1/3P_3$ to simultaneously determine H_ρ as well as the spatial scale for the loop lateral expansion (Van Doorsselaere, Birtill, and Evans, 2009).

Fundamental or global sausage modes together with their first overtones were also detected in flaring loops with NoRH (Nakariakov, Melnikov, and Reznikova, 2003; Melnikov *et al.*, 2005) and in cool Hα loops (Srivastava *et al.*, 2008). In the former, $P_1/2P_2$ was found to be ≈ 0.82 with $P_1 \approx 14 - 17$ seconds and $P_2 \approx 8 - 11$ seconds. In the latter, a value of ≈ 0.84 was found for $P_1/2P_2$ with $P_1 \approx 587$ seconds and $P_2 \approx 349$ seconds. Despite these measurements, making use of $1-P_1/2P_2$ pertinent to sausage modes is not as popular as in the case of standing kink modes. Rather, more attention was paid to the cutoff loop width-to-length ratio, only beyond which can trapped standing sausage modes be supported. For instance, capitalizing on this cutoff, Aschwanden, Nakariakov, and Melnikov (2004) deduced that the sausage oscillations measured using radio instruments with observing frequencies ranging from 100 MHz to 1 GHz prior to the 2000s were likely to be confined in a loop segment instead of perturbing the entire loop. For loops with width-to-length ratios smaller than the cutoff, sausage modes are no longer trapped but become leaky. However, this change of nature does not mean that these modes are not observationally irrelevant: the damping timescale of the leaky modes can be sufficiently longer than their periods, making their detection possible in oscillating signals of coronal loops with realistic parameters, as shown recently by Nakariakov, Hornsey, and Melnikov (2012).

The effects of a field-aligned flow in coronal loops on the standing modes that they support were often neglected. While this is justifiable when the flow speeds are well below the Alfvén speed, as was assessed for kink modes supported by thin tubes (Ruderman, 2010), loop flows are not necessarily always weak. In fact, speeds in the Alfvénic regime ($\approx 10^3$ km s^{-1}) associated with explosive events have been reported (*e.g.* Innes, McKenzie, and Wang, 2003; Harra *et al.*, 2005). Alternatively, as was pointed out by Terradas *et al.* (2011), speeds of similar magnitude can be independently inferred from the spatial distributions of the phases associated with standing kink modes along loops such as those reported by Verwichte, Foullon, and Van Doorsselaere (2010) using TRACE and SOHO data. If the effects of such a strong flow are neglected, then the loop magnetic field strength would be seriously underestimated with the standard seismological practice, by a factor of three to be precise (Terradas *et al.*, 2011).

The present study is intended to provide a comprehensive investigation into the flow effects on standing modes supported by coronal loops modeled by a zero-β slab, where β is the ratio of the thermal to the magnetic pressure. Similar studies on cylinder-supported kink modes were carried out by Ruderman (2010) and more recently by Erdélyi, Hague, and Nelson (2013), both adopting the thin-tube limit and assuming weak flow speeds well below the Alfvén speed.

In the slab case, the most relevant one seems to be that by Macnamara and Roberts (2011; hereafter MR11) where an exhaustive analytical study on the period ratio $[P_1/2P_2]$ for static zero-β slabs was conducted. Our previous work (Li, Habbal, and Chen, 2013) (hereafter Article I) adopted also a slab geometry, and examined in detail how the flows, which are allowed to reach the Alfvénic range, influence $P_1/2P_2$ of both kink and sausage modes for slabs with arbitrary width-to-length ratios in both a coronal and a photospheric environment. The present study extends both MR11 and Article I in three ways: First, as observations are not restricted to the first overtone but show the existence of even higher ones, we will examine how the flows affect overtones with n being up to four. By doing this, we will show that measuring simultaneously three periods will lead one to determine the density contrast $[\rho_0/\rho_{\rm e}]$ and the internal Alfvén Mach number $[M_A]$. Second, as shown by Article I, the flow effects may be best brought out by examining, say, whether the minimum P_1/nP_n is subject to the lower limits expected for static slabs. We will extend MR11 to overtones of arbitrary order $[n]$ by establishing the lower limits of P_1/nP_n for static slabs: while they are to be analytically derived for slabs with an Epstein density profile, we show that they also hold for slabs with density profiles taking a step-function form. Third, regarding coronal sausage oscillations, Article I showed that the most prominent influence a flow has is to increase the critical width-to-length ratio $[(w/L)_{\rm cutoff}]$ required for standing sausage modes to be trapped. We will extend this by conducting a parameter study of $(w/L)_{\rm cutoff}$, and come up with an analytical fit that depends only on $\rho_0/\rho_{\rm e}$ and M_A. This simple formula will then be applied to demonstrate how the simple fact that a standing sausage mode exists in a coronal loop can constrain the combination of $\rho_0/\rho_{\rm e}$ and M_A. In addition, it allows us to further the study by Aschwanden, Nakariakov, and Melnikov (2004) of the partial sausage modes.

This article is organized as follows: Section 2 examines static slabs, with the purpose of establishing the behavior of P_1/nP_n in general, and its lower limit in particular. Then Section 3 examines in detail how introducing a field-aligned flow affects standing modes, with particular attention paid to the period ratios for kink and sausage modes alike, as well as the cutoff width-to-length ratio for sausage modes. Section 4 summarizes the present study.

2. The Static Case

Let us start with a static slab of length L aligned with the z-axis in a Cartesian geometry. The background magnetic field $[\boldsymbol{B}_0 = B_0\hat{\boldsymbol{z}}]$ is uniform, whereas the background density $[\rho(x)]$ is structured along the x-direction, resulting in a non-uniform Alfvén speed $[v_{\rm A}(x) = \sqrt{B_0^2/4\pi\rho(x)}]$. Two forms of $\rho(x)$ are examined: one is the Epstein profile (Landau, and Lifshitz, 1958) while the other is a step-function form. The former enables a fully analytic exploration of the period ratios of the standing modes supported by static slabs (*e.g.* Nakariakov and Roberts, 1995b; Cooper, Nakariakov, and Williams, 2003; Pascoe, Nakariakov, and Arber, 2007; Macnamara and Roberts, 2011). Exploiting this analytical tractability, we will derive the expressions for the period ratios $[P_1/nP_n]$ associated with

overtones of arbitrary order [n], their approximations in a number of physically interesting limits, and their lower limits. The purpose is to show that, while these properties are established for this particular profile, they apply also to the case of a step-function profile, which is easier to implement numerically, and which is the profile to be used when field-aligned flows are introduced.

The Epstein profile is

$$\frac{\rho(x)}{\rho_0} = r^{-1} + (1 - r^{-1})\mathrm{sech}^2\left(\frac{x}{d}\right). \tag{1}$$

As shown in Figure 1, this density profile continuously connects the asymptotic value [ρ_e] to a maximum [ρ_0] over a characteristic spatial scale [d]. The ratio [r] evaluates the density contrast [ρ_0/ρ_e]. Strictly speaking, what Equation (1) describes is the symmetric Epstein profile, a particular class of the more general Epstein profiles. It is still referred to as "the Epstein profile" throughout only for brevity. As for the step-function form, it simply reads

$$\rho(x) = \begin{cases} \rho_\mathrm{e}\ , & |x| > d \\ \rho_0\ . & |x| < d \end{cases} \tag{2}$$

In either case, we define $v_{\mathrm{A}i}$ as $B_0/\sqrt{4\pi\rho_i}$ with $i = 0,\ \mathrm{e}$. From transverse force balance in zero-β MHD it follows that

$$\rho_0/\rho_\mathrm{e} = v_\mathrm{Ae}^2/v_\mathrm{A0}^2. \tag{3}$$

Moreover, regardless of the density profile, the half-width of the slab is taken to be d, resulting in the definition of the aspect ratio as d/L.

We restrict ourselves to trapped linear waves that propagate only in the x–z-plane. Let ω and k represent their angular frequency and longitudinal wavenumber. The phase speed [v_ph] is defined as $v_\mathrm{ph} = \omega/k$. For standing modes the wavenumber [k] is quantized

$$k_n = \frac{n\pi}{L}, n = 1, 2, \ldots \tag{4}$$

This expression is valid for both the fundamental mode [$n = 1$] and its overtones [$n \geq 2$]. The period ratios [P_1/nP_n] are then simply

$$\frac{P_1}{nP_n} = \frac{k_n v_{\mathrm{ph},n}}{nk_1 v_{\mathrm{ph},1}} = \frac{v_{\mathrm{ph},n}}{v_{\mathrm{ph},1}}\ , \tag{5}$$

where $v_{\mathrm{ph},n} \equiv v_\mathrm{ph}(k_n)$ is the phase speed evaluated at k_n. Hence the k-dependence of v_ph translates into the dependence on the aspect ratio [d/L] of the period ratios [P_1/nP_n]. Not surprisingly, P_1/nP_n depends also on ρ_0/ρ_e. Actually, P_1/nP_n is determined by these two parameters, and these two only.

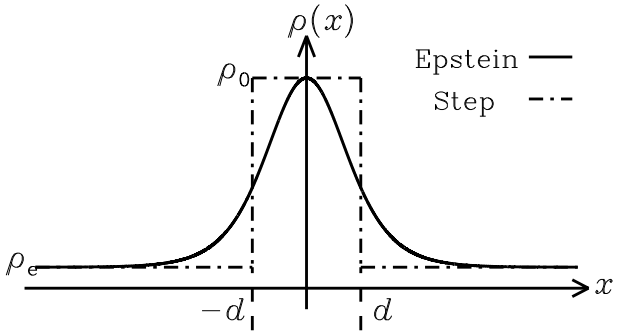

Figure 1. The transverse density inhomogeneity of a magnetic slab. The solid and dash–dotted curves correspond to the Epstein and step function profiles, respectively.

2.1. The Epstein Profile Slab

In this case, for kink waves the dispersion relation reads (*e.g.* Nakariakov and Roberts, 1995b)

$$\frac{v_{\rm ph}^2}{v_{\rm A0}^2} = 1 + \frac{\sqrt{r^{-2} + 4k^2d^2 - 4k^2d^2r^{-1}} - r^{-1}}{2k^2d^2}\ , \tag{6}$$

which leads to a general expression for the period ratios

$$\left(\frac{P_1}{nP_n}\right)^2 = \frac{1}{n^2}\left(\frac{\dfrac{2n^2\pi^2d^2}{L^2} - r^{-1} + \sqrt{r^{-2} + \dfrac{4n^2\pi^2d^2}{L^2} - \dfrac{4n^2\pi^2d^2}{L^2}r^{-1}}}{\dfrac{2\pi^2d^2}{L^2} - r^{-1} + \sqrt{r^{-2} + \dfrac{4\pi^2d^2}{L^2} - \dfrac{4\pi^2d^2}{L^2}r^{-1}}}\right)\ . \tag{7}$$

By deriving Equation (7) we have presented an expression for P_1/nP_n that is valid for overtones of arbitrary order. Specializing to the first overtone ($n = 2$), one readily recovers Equation (20) in MR11. We note, however, the symbol L therein is equivalent to $L/2$ in this study.

Let us proceed by examining the slender- and wide-slab limits. In the former case [$d/L \ll 1$], the period ratio P_1/nP_n as given by Equation (7) may be satisfactorily approximated by

$$\frac{P_1}{nP_n} \approx 1 - \frac{\pi^2d^2\mu_2}{2L^2}\left(n^2-1\right) - \frac{\pi^4d^4\mu_2^2}{8L^4}\left(n^4+2n^2-3\right)\ , \qquad \mu_2 \equiv \left(\frac{v_{\rm Ae}^2}{v_{\rm A0}^2} - 1\right)^2\ , \tag{8}$$

When the opposite is true [$d/L \gg 1$], P_1/nP_n may be expressed as

$$\frac{P_1}{nP_n} \approx 1 - \frac{L\mu_1}{2\pi d}\left(1 - \frac{1}{n}\right) + \frac{L^2\mu_1^2}{4\pi^2d^2}\left(\frac{3}{2} - \frac{1}{n} - \frac{1}{2n^2}\right)\ , \qquad \mu_1 \equiv \sqrt{1 - \frac{v_{\rm A0}^2}{v_{\rm Ae}^2}}. \tag{9}$$

Equations (8) and (9) generalize Equations (24) and (25) in MR11 by providing the expressions for arbitrary n.

The lower limit of period ratios P_1/nP_n turns out to be of particular interest, and can be derived in two steps. First, one notices that P_1/nP_n at any positive d/L decreases with increasing r as long as $r > 1$. Second, P_1/nP_n in the limit $r \to \infty$ has the asymptotic form

$$\lim_{r\to\infty} \frac{P_1}{nP_n} = \sqrt{\frac{\dfrac{\pi d}{L} + \dfrac{1}{n}}{\dfrac{\pi d}{L} + 1}} > \frac{1}{\sqrt{n}} \tag{10}$$

for any finite aspect ratio $[d/L]$. Hence the lower limit for P_1/nP_n is $1/\sqrt{n}$, attained when the density contrast approaches infinity and the aspect ratio approaches zero.

For sausage waves, the dispersion relation reads (*e.g.* Pascoe, Nakariakov, and Arber, 2007; Inglis *et al.*, 2009)

$$\frac{v_{\rm ph}^2}{v_{\rm A0}^2} = 1 + \frac{3\sqrt{9r^{-2} - 8r^{-1} + 4k^2d^2 - 4k^2d^2r^{-1}} - 9r^{-1} + 4}{2k^2d^2}. \tag{11}$$

Consequently, one finds a general expression for the period ratios

$$\left(\frac{P_1}{nP_n}\right)^2 = \frac{1}{n^2}\left(\frac{\dfrac{2n^2\pi^2d^2}{L^2} + 4 - 9r^{-1} + 3\sqrt{9r^{-2} - 8r^{-1} + \dfrac{4n^2\pi^2d^2}{L^2} - \dfrac{4n^2\pi^2d^2}{L^2}r^{-1}}}{\dfrac{2\pi^2d^2}{L^2} + 4 - 9r^{-1} + 3\sqrt{9r^{-2} - 8r^{-1} + \dfrac{4\pi^2d^2}{L^2} - \dfrac{4\pi^2d^2}{L^2}r^{-1}}}\right), \tag{12}$$

which generalizes Equation (33) in MR11, where only the first overtone is concerned, to overtones with arbitrary order $[n]$.

Concerning sausage waves, a number of analytically tractable properties are of interest. The first concerns the dispersion behavior in the wide-slab limit $[d/L \gg 1]$, in which case P_1/nP_n reads

$$\frac{P_1}{nP_n} \approx 1 - \frac{3L\mu_1}{2\pi d}\left(1 - \frac{1}{n}\right) - \frac{L^2}{\pi^2d^2}\left(1 - \frac{1}{n^2}\right) + \frac{9L^2\mu_1^2}{4\pi^2d^2}\left(\frac{3}{2} - \frac{1}{n} - \frac{1}{2n^2}\right), \tag{13}$$

where μ_1 is the same as in Equation (9). It is noteworthy that Equation (36) in MR11 is a special case $[n = 2]$ of Equation (13). The second concerns the lower bound that P_1/nP_n may attain. One first notices that P_1/nP_n as a function of $(d/L, r)$ decreases with r at any positive d/L when $r > 1$. Furthermore, when the density contrast $r \to \infty$, one finds that

$$\lim_{r\to\infty} \frac{P_1}{nP_n} = \sqrt{\frac{\dfrac{2\pi^2d^2}{L^2} + \dfrac{4}{n^2} + \dfrac{6\pi d}{nL}}{\dfrac{2\pi^2d^2}{L^2} + 4 + \dfrac{6\pi d}{L}}} > \frac{1}{n}\,. \tag{14}$$

Finally, a cutoff wavenumber exists (*e.g.* Pascoe, Nakariakov, and Arber, 2007; Inglis *et al.*, 2009)

$$kd = \sqrt{\frac{2}{r-1}}\ , \tag{15}$$

below which the waves are no longer trapped. Going a step further, one finds an aspect ratio cutoff

$$(d/L)_{\rm cutoff} = \frac{1}{\pi}\sqrt{\frac{2}{r-1}}. \tag{16}$$

2.2. The Step Function Slab

In this case the dispersion relation reads (*e.g.* Edwin and Roberts, 1982, 1988)

$$\cot\left(kd\sqrt{\frac{v_{\rm ph}^2 - v_{\rm A0}^2}{v_{\rm A0}^2}}\right) = \frac{v_{\rm Ae}}{v_{\rm A0}}\sqrt{\frac{v_{\rm ph}^2 - v_{\rm A0}^2}{v_{\rm Ae}^2 - v_{\rm ph}^2}} \tag{17}$$

for kink waves, and

$$\tan\left(kd\sqrt{\frac{v_{\rm ph}^2 - v_{\rm A0}^2}{v_{\rm A0}^2}}\right) = -\frac{v_{\rm Ae}}{v_{\rm A0}}\sqrt{\frac{v_{\rm ph}^2 - v_{\rm A0}^2}{v_{\rm Ae}^2 - v_{\rm ph}^2}} \tag{18}$$

for sausage waves. As in the case where the Epstein profile is adopted, for sausage waves to be trapped, the longitudinal wavenumber has to be larger than a cutoff (*e.g.* Edwin and Roberts, 1988)

$$kd = \frac{\pi}{2}\sqrt{\frac{1}{r-1}}. \tag{19}$$

Consequently, a cutoff aspect ratio exists

$$(d/L)_{\rm cutoff} = \frac{1}{2}\sqrt{\frac{1}{r-1}}\ , \tag{20}$$

only beyond which can standing sausage modes be trapped.

Evaluating the period ratios $[P_1/nP_n]$ in the step function case can in principle be done in the same way as in the previous case, the only difference being that the phase speed $[v_{\rm ph}]$ has to be found numerically. Having found $v_{\rm ph}$ as a function of the dimensionless longitudinal wavenumber $[kd]$, one readily finds P_1/nP_n by employing Equation (4).

2.3. Comparing Slabs with Two Different Density Profiles

Now let us evaluate how sensitively the period ratios depend on the profile that the density inhomogeneity adopts. In addition, let us examine whether the lower limits of the period ratios are different for different choices of the density profiles.

Figure 2 compares the period ratios $[P_1/nP_n]$ for standing kink modes for the Epstein (solid curves) and step-function density profiles (dashed). Here the density contrast $[\rho_0/\rho_e]$ is 16, arbitrarily chosen but observationally realistic. Consider the solid curves first, in which case the behavior of P_1/nP_n can be readily understood with the aid of the approximate expressions valid for the Epstein profile. As expected from Equation (8), when d/L is small, P_1/nP_n starts from unity, regardless of the values of n and density contrast $[\rho_0/\rho_e]$. With increasing d/L, P_1/nP_n decreases to its minimum, and then approaches unity from below as would be expected from Equation (9). Comparing the dashed with the solid curves, one sees that choosing different density profiles does not make a qualitative difference. In fact, the curves corresponding to the same order $[n]$ differ little from one another, with P_1/nP_n being slightly lower in the step function case.

Can the slight difference in P_1/nP_n be reflected in their minima $[(P_1/nP_n)_{\min}]$ at different values of density contrast? This is examined in Figure 3 where the Alfvén speed ratio $[v_{Ae}/v_{A0}]$ ranges from 2 to 32. In addition to $(P_1/nP_n)_{\min}$ for the two profiles, the lower limit $\sqrt{1/n}$ as expected from Equation (10) is plotted by the dash–dotted lines for comparison. One can see that at all of the examined v_{Ae}/v_{A0}, $(P_1/nP_n)_{\min}$ for one profile differs little from that for the other. In fact, a fractional change of at most 3.5 % is found for all the examined n. Looking further at the period ratios at large v_{Ae}/v_{A0}, one sees that $(P_1/nP_n)_{\min}$ tends to the lower bound $[\sqrt{1/n}]$. Even though it is analytically established for an Epstein profile, it holds for the step-function profile as well.

Moving on to the standing sausage modes pertinent to static slabs, Figure 4 examines the dependence on the slab aspect ratio $[d/L]$ of the period ratios $[P_1/nP_n]$ with n being up to four. It can be seen that the profile-associated difference in P_1/nP_n is more pronounced than for standing kink modes, with the step-function profile corresponding to lower P_1/nP_n. This difference decreases with increasing d/L. The fractional change in P_1/nP_n for the step-function profile relative to the Epstein one is found to be up to 8 %, 10 %, 11 % for $n = 2, 3,$ and 4, respectively. In this regard, one would have to measure the periods with an accuracy of better than ≈ 5 % to tell which profile better describes the density structuring. One further notes that at this density contrast, P_1/nP_n for both profiles remains substantially larger than $1/n$, the expected lower bound as given by Equation (14). On the other hand, one can see that the cutoff aspect ratios $[(d/L)_{\rm cutoff}]$ associated with the two profiles are not significantly different, reading 0.116 (0.129) for the Epstein (step-function) profile. Actually, analytically expected values for these, Equations (16) and (20), yield that the ratio between the two is $2\sqrt{2}/\pi \approx 0.9$.

Figure 5 examines how the minima of P_1/nP_n for standing sausage modes depend on the choice of the density profiles for Alfvén-speed ratios v_{Ae}/v_{A0} ranging from 2 to 32. For comparison, the lower bounds $[1/n]$ expected analytically from Equation (14) are plotted by the dash–dotted lines. One can see that while the $(P_1/nP_n)_{\min}$ curves for the step-function profile (the dashed curves) lie generally below those for the Epstein profile (solid), the difference between them decreases with increasing v_{Ae}/v_{A0}. The fractional changes between the two, the step function case relative to the Epstein one, are typically 10 % for all values

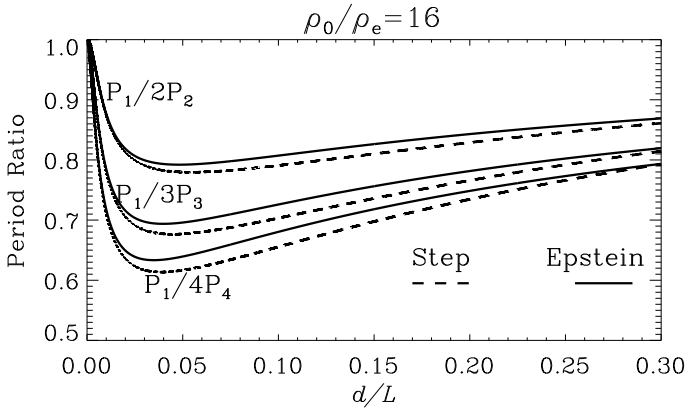

Figure 2. Effects of transverse density profile on standing kink modes supported by static coronal slabs. Period ratios $[P_1/nP_n(n = 2, 3, 4)]$ are displayed as functions of aspect ratio $[d/L]$ for a density contrast $\rho_0/\rho_e = 16$. The solid and dashed lines correspond to the Epstein and step-function profiles, respectively.

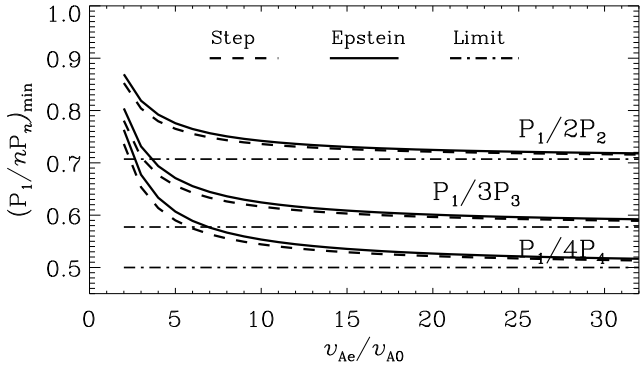

Figure 3. Effects of transverse density profile on standing kink modes supported by static coronal slabs. Minima of period ratios $[(P_1/nP_n)_{\min}(n = 2, 3, 4)]$ are displayed as functions of the Alfvén speed ratio $[v_{Ae}/v_{A0} = (\rho_0/\rho_e)^{1/2}]$. The solid and dashed lines stand for the Epstein and step-function profiles, respectively. In addition, the dot–dashed lines represent $1/\sqrt{n}$, the lower limits of period ratios P_1/nP_n analytically derived for the Epstein profile (Equation (10)).

of n considered when $v_{Ae}/v_{A0} < 15$, but drop below 6 % when $v_{Ae}/v_{A0} > 20$. For both profiles, $(P_1/nP_n)_{\min}$ tends to $1/n$ when v_{Ae}/v_{A0} is sufficiently large, meaning once again that while this lower bound is established analytically for the Epstein profile, it is valid also for the step-function one.

3. The Flowing Case

In this section, we will examine the effect of field-aligned flow on the standing modes supported by a magnetic slab. For the ease of numerical implementation, a step-function form is chosen for the transverse density profile, as well as for

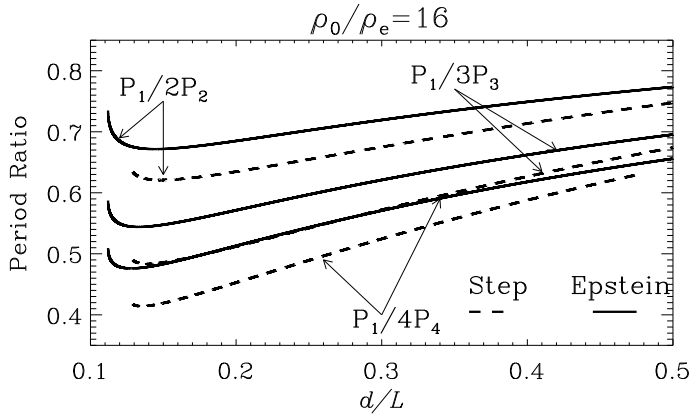

Figure 4. Effects of transverse density profile on standing sausage modes supported by static coronal slabs. Period ratios $[P_1/nP_n(n = 2, 3, 4)]$ are displayed as functions of aspect ratio $[d/L]$ for a density contrast $\rho_0/\rho_e = 16$. The solid and dashed lines correspond to the Epstein and step function profiles, respectively.

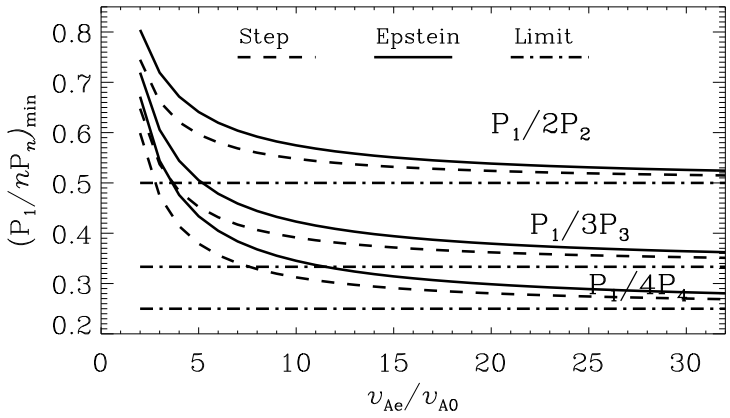

Figure 5. Effects of transverse density profile on standing sausage modes supported by static coronal slabs. Minima of period ratios $[(P_1/nP_n)_{\rm min}(n = 2, 3, 4)]$ are displayed as functions of the Alfvén speed ratio $[v_{\rm Ae}/v_{\rm A0} = (\rho_0/\rho_e)^{1/2}]$. The solid and dashed lines stand for the Epstein and step-function profiles, respectively. The dash–dotted lines represent $1/n$, the lower limits of P_1/nP_n analytically expected for the Epstein profile.

the speed profile. The flow speed external to the slab $[U_e]$ is taken to be zero, but the internal flow $[U_0]$ is in general finite, and this is conveniently measured in units of the internal Alfvén speed. In other words, $U_0 \equiv M_{\rm A} v_{\rm A0}$ with $M_{\rm A}$ being the internal Alfvénic Mach number.

The dispersion relation of trapped linear waves supported by a cold slab with field-aligned flow can be found by letting the sound speeds approach zero in the more general versions (*e.g.* Nakariakov and Roberts, 1995a). One finds

$$\frac{\rho_e}{\rho_0}\frac{n_0}{|m_e|}\frac{v_{\rm Ae}^2 - v_{\rm ph}^2}{v_{\rm A0}^2 - (v_{\rm ph} - U_0)^2} = \left\{ \begin{array}{c} -\tan \\ \cot \end{array} \right\} (n_0 d) \ . \qquad (21)$$

Here $m_{\rm e}$ (n_0) plays the role of the transverse wave number outside (inside) the slab, defined as

$$m_{\rm e}^2 = \frac{v_{\rm Ae}^2 - v_{\rm ph}^2}{v_{\rm Ae}^2} k^2 \ , \qquad n_0^2 = \frac{\left(v_{\rm ph} - U_0\right)^2 - v_{\rm A0}^2}{v_{\rm A0}^2} k^2 \ . \tag{22}$$

In addition, the upper/lower case in Equation (21) is for kink/sausage modes.

Finding the period ratios of standing modes supported by a flowing slab is not as straightforward as in the static case. Nevertheless, as detailed in Article I, a simple graphical means can be used for this purpose by capitalizing on the ω–k diagrams. The component propagating waves in a pair to form standing modes correspond to two curves in an ω–k diagram, a horizontal cut with a constant ω would intersect the two at two points. If the separation between the two points is $2\pi/L$, then one finds the fundamental mode. If it is $2n\pi/L$, one finds the $(n-1)^{\rm th}$ overtone. Let the angular frequency of the fundamental mode be denoted by ω_1, that of the $(n-1)^{\rm th}$overtone by ω_n, the period ratio is then simply $P_1/nP_n = \omega_n/n\omega_1$. In the flowing case, in addition to the density contrast $[\rho_0/\rho_{\rm e}]$ and aspect ratio $[d/L]$ of the considered slab, the period ratios $[P_1/nP_n]$ depend also on the internal Alfvén Mach number $[M_A = U_0/v_{A0}]$.

3.1. Standing Kink Modes

Figure 6 presents the dependence on the slab aspect ratio $[d/L]$ of the period ratios $[P_1/nP_n]$ for standing kink modes. An Alfvén Mach number $M_A = 0.6$ is chosen (the solid lines) for the magnitude of the internal flow. The static results are also shown here by the dotted lines for comparison. One may see that while the trend for the P_1/nP_n profiles is the same in the flowing case as in the static one, the effect of the flow is substantial. Take the minimum value that P_1/nP_n may attain for instance. For $n = [2,\ 3,\ 4]$, this minimum reads $[0.78,\ 0.676,\ 0.614]$ in the static case, but reads $[0.711,\ 0.587,\ 0.514]$ in the case where $M_A = 0.6$, amounting to a fractional decrease of $[8.8\,\%,\ 13.2\,\%,\ 16.3\,\%]$. Furthermore, the aspect ratios where the minima are attained tend to decrease with n, but at a given n they tend to increase by a substantial amount in the flowing case relative to the static one. When $M_A = 0$, they read $[0.053, 0.045, 0.039]$ for $n = [2, 3, 4]$. The corresponding values are $[0.073, 0.059, 0.05]$ when $M_A = 0.6$.

The effect of the flow magnitude on the period ratios for standing kink modes is better illustrated by Figure 7, which presents the dependence on the Alfvén Mach number $[M_A]$ of the minimal period ratios $[(P_1/nP_n)_{\rm min}]$. Two density contrasts, $\rho_0/\rho_{\rm e} = 16$ and 256, are examined and plotted by the dashed and solid lines, respectively. The horizontal bars on the right of the panel represent the lower bound $[\sqrt{1/n}]$ for static slabs. One finds that the introduction of flow reduces $(P_1/nP_n)_{\rm min}$ as a whole. When the density contrast $[\rho_0/\rho_{\rm e}]$ is 256 for n being 2 (3, 4) the minimum of P_1/nP_n reduces from 0.73 (0.6, 0.53) in the static case to 0.63 (0.48, 0.4) at $M_A = 0.8$, amounting to a fractional reduction of 13.7 % (20.3 %, 24.5 %). At a lower density contrast $\rho_0/\rho_{\rm e} = 16$, the flow effect is even stronger, as demonstrated by that relative to the static case, the fractional

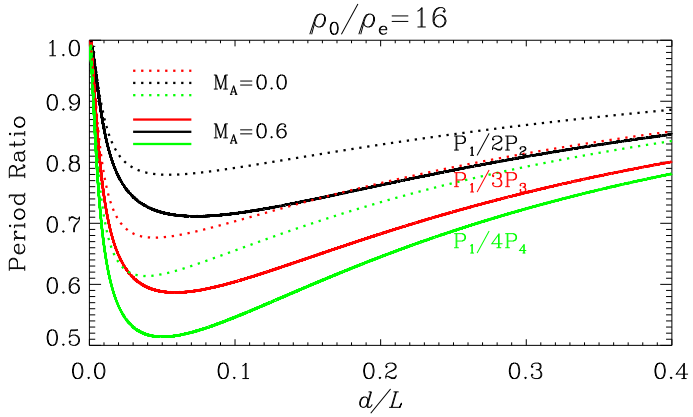

Figure 6. Effects of flow on period ratios $[P_1/nP_n]$ for standing kink modes at a density ratio $\rho_0/\rho_e = 16$. Here the period ratios $[P_1/nP_n]$ as functions of aspect ratio $[d/L]$ are given for a flowing cold slab with an internal Alfvén Mach number $M_A = 0.6$ (the solid curves), and also for a static slab (the dotted curves) for comparison. The black, red, and green curves describe the period ratios $P_1/2P_2$, $P_1/3P_3$, and $P_1/4P_4$.

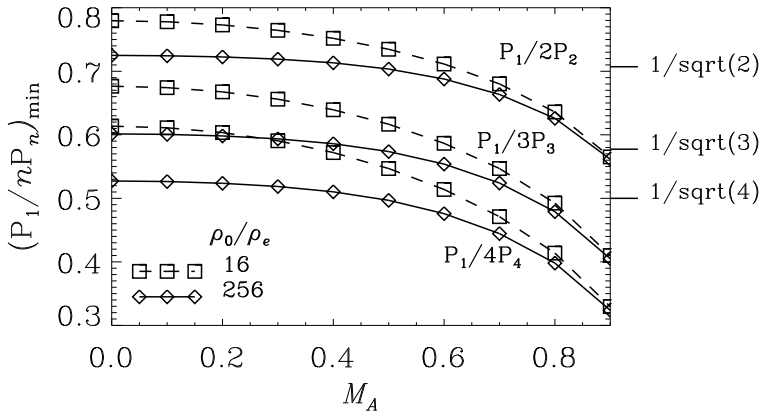

Figure 7. Minima of period ratios $[(P_1/nP_n)_{\min}\ (n = 2, 3, 4)]$ as functions of internal Alfvén Mach numbers $[M_A]$. Two density contrasts $[\rho_0/\rho_e]$, 16 and 256, are represented by the dashed and solid curves, respectively. Besides, the symbols (open boxes and diamonds) represent specific computations. The horizontal bars on the right correspond to $1/\sqrt{n}$, the lower bound analytically expected for static slabs.

reduction in the minimum of $P_1/2P_2$, $P_1/3P_3$, and $P_1/4P_4$ at $M_A = 0.8$ reads 18.5 %, 27.2 % and 32.6 %, respectively. Besides, while for static slabs P_1/nP_n is subject to the lower limit $1/\sqrt{n}$, this is no longer the case for flowing slabs.

The feature that persists in Figure 7, regardless of M_A and ρ_0/ρ_e, is that P_1/nP_n tends to decrease with increasing n. The values $P_1/2P_2 = 0.99$ and $P_1/3P_3 = 0.965$ measured by Van Doorsselaere, Birtill, and Evans (2009) for a TRACE 171Å loop on 13 May 2001 agree with this tendency. As for the extremely small deviation of P_1/nP_n from unity, it may come from the small aspect ratio of EUV loops, or may be due to the longitudinal structuring in loop

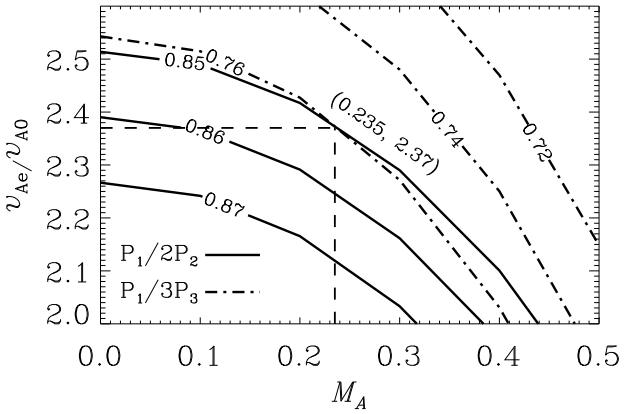

Figure 8. Contours of period ratios [$P_1/2P_2$ (solid) and $P_1/3P_3$ (dash–dotted)] with respect to M_A and $v_{\rm Ae}/v_{\rm A0}$ at an aspect ratio $d/L = 0.05$. The contours for $P_1/2P_2$ ($P_1/3P_3$) are equally spaced by 0.01 (0.02).

density as well as magnetic field strength as suggested by Van Doorsselaere, Birtill, and Evans (2009). On the other hand, the NoRH loop that underwent standing kink oscillations as measured by Kupriyanova, Melnikov, and Shibasaki (2013) yields values for $P_1/2P_2$ to be 0.83 and for $P_1/3P_3$ to be 0.91, at variance with the afore-mentioned tendency. However, a closer inspection of Figure 5 therein shows that the period 11.5 seconds regarded as the second overtone may correspond in fact to even higher overtones, for the spatial distribution of the associated spectral power does not clearly show a signature with three peaks between the two footpoints. In contrast, the periods 31.2 seconds and 21.3 seconds correspond to distributions of spectral power concentrated near the loop apex and close to footpoints, respectively, indeed in line with the expectation that these are for the fundamental and the 1st overtone. If one tentatively attributes 11.5 seconds to the third overtone, then one finds that $P_1/4P_4 = 0.68$, which no longer contradicts the tendency for P_1/nP_n to decrease with n. Given the uncertainties in interpreting this 11.5-second period, the final answer certainly awaits a dedicated calculation, which should take into account both longitudinal and transverse structuring. We note that the latter is necessary given that the NoRH loop in question has an aspect ratio of 0.19 for which the dispersion due to finite aspect ratios cannot be neglected.

That a field-aligned flow may have substantial effects on the period ratios for standing kink modes leads naturally to a diagnostic tool for deducing the flow magnitude. This is illustrated in Figure 8, where the contours of period ratios $P_1/2P_2$ (the solid curves) and $P_1/3P_3$ (dash–dotted) are shown as a function of the Alfvén Mach number [$M_{\rm A}$] and the Alfvén speed ratio [$v_{\rm Ae}/v_{\rm A0}$], at a given aspect ratio [d/L]. For illustrative purposes, the results shown are for d/L being 0.05, which is not unrealistic but lies within the range deduced for TRACE 171Å loops (Ofman and Aschwanden, 2002, Table 1). One sees that at a given density ratio, both $P_1/2P_2$ and $P_1/3P_3$ decrease with increasing M_A. Likewise, at a given M_A, both $P_1/2P_2$ and $P_1/3P_3$ decrease with $v_{\rm Ae}/v_{\rm A0}$. Although following the same pattern, the two sets of contours may intersect at a series of points:

the solid contour corresponding to $P_1/2P_2 = 0.85$ intersects the dash-dotted one corresponding to $P_1/3P_3 = 0.76$ at $(M_A, v_{\rm Ae}/v_{\rm A0}) = (0.235, 2.37)$. So the point that we make here is that if a loop undergoes standing kink oscillations, and if the oscillating signals contain periods of both the fundamental and its first and second overtones, then with the measured periods one can readily derive simultaneously the density contrast of the loop with its surroundings and the internal Alfvén Mach number: Neither of these two is easy to measure directly from an observational standpoint. Actually, if from observations one sees also the third overtone, then the measured $P_1/4P_4$ can provide an additional means for checking the quality of the derived flow magnitude and density contrast. For instance, at this afore-mentioned combination of $[M_A, v_{\rm Ae}/v_{\rm A0}]$, the theoretically expected $P_1/4P_4$ at the given d/L would be ≈ 0.7, meaning that the amount by which the measured $P_1/4P_4$ deviates from this theoretical value serves as a natural uncertainty measure.

3.2. Standing Sausage Modes

Now we examine the standing sausage modes supported by a flowing slab. Figure 9 presents P_1/nP_n with n ranging from 2 to 4 as a function of aspect ratio $[d/L]$ at a density contrast of $\rho_0/\rho_{\rm e} = 256$. To bring out the flow effect, the static case (dotted lines) is also presented in addition to a flowing case where the Alfvén Mach number $[M_A]$ is 0.6. One can see that all period ratios $[P_1/nP_n]$ decrease with the introduction of the flow. For instance, at $d/L = 0.2$ the period ratios with n being $[2, 3, 4]$ reduce from $[0.62, 0.5, 0.44]$ in the static case to [0.567, 0.434, 0.372] in the flowing case. The fractional reduction is therefore $[8.7\,\%, 13.4\,\%, 16.2\,\%]$. One can see that for a density contrast as large as 256, P_1/nP_n close to the cutoff aspect ratio in the static case is close to their lower limits $[1/n]$ established by Equation (14). However, while at a given aspect ratio the flow reduces P_1/nP_n to a substantial extent, the minimal P_1/nP_n in the flowing case is similar to that in the static case, the reason being that the cutoff aspect ratio $[(d/L)_{\rm cutoff}]$ shifts towards larger values when a flow is present. One finds that in the static case $(d/L)_{\rm cutoff}$ is 0.031. However it is 0.148 in the case where $M_A = 0.6$, amounting to an increase by a factor of 3.8.

That $(P_1/nP_n)_{\rm min}$ changes little even in the presence of a substantial flow raises the question of how to explain the observed period ratios as reported by Nakariakov, Melnikov, and Reznikova (2003) for NoRH flaring loops and by Srivastava *et al.* (2008) for cool Hα loops. Recall that in the former $P_1/2P_2$ reads 0.82 at an aspect ratio $d/L = 0.12$. Figure 10 examines what we derive for $P_1/2P_2$ at this aspect ratio for an extensive range of v_{Ae}/v_{A0} and M_A. The contours of $P_1/2P_2$ are equally spaced by 0.01. One can see that the lower-right portion is blank, for at those given v_{Ae}/v_{A0} trapped sausage modes are not allowed at this aspect ratio. Looking at the values of $P_1/2P_2$, one sees that $P_1/2P_2$ tends to decrease with M_A at a given v_{Ae}/v_{A0}, and this tendency is stronger for larger v_{Ae}/v_{A0}. Nevertheless, in the whole parameter range $P_1/2P_2$ varies by no more than $\approx 12\,\%$ if one compares their values at the lower-left corner with those at the upper right one. More importantly, they never exceed ≈ 0.6, which is considerably smaller than the observed value. Actually, given that

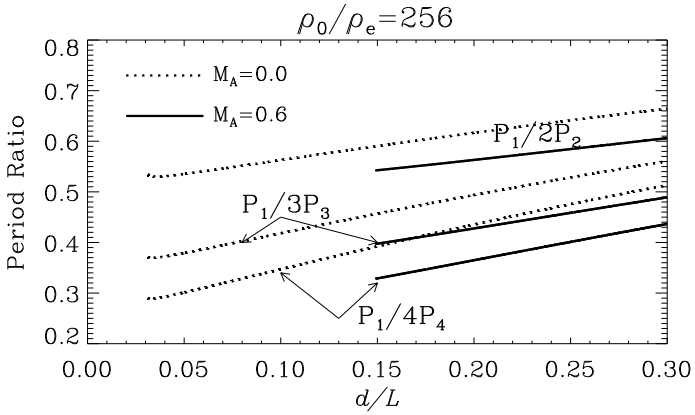

Figure 9. Period ratios $[P_1/nP_n\ (n = 2,\ 3,\ 4)]$ as functions of aspect ratio $[d/L]$ for a static (dotted lines) and a flowing slab (solid).

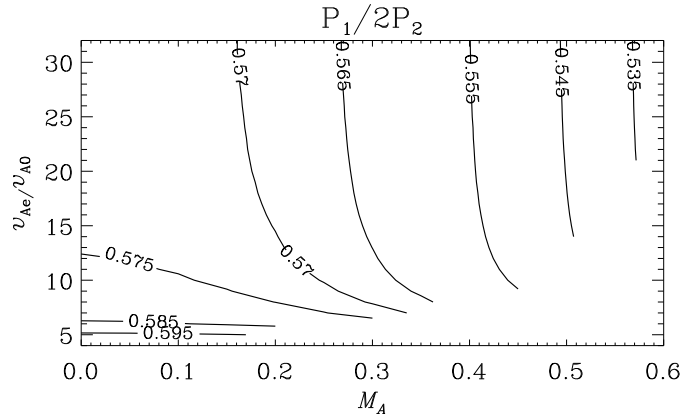

Figure 10. Period ratio $[P_1/2P_2]$ of standing sausage modes for flowing slabs with an aspect ratio of 0.12 as a function of the Alfvén speed ratio $[v_{Ae}/v_{A0}]$ and internal Alfvén Mach number $[M_A]$. This aspect ratio corresponds to the flaring loop that underwent a standing sausage oscillation on 12 January 2000 as measured with NoRH (Nakariakov, Melnikov, and Reznikova, 2003).

the theoretically expected values are smaller than the observed, introducing a flow makes the comparison even more undesirable since a flow would decrease rather than increase $P_1/2P_2$. A similar study at $d/L = 0.03$, pertinent to the Hα loops reported by Srivastava *et al.* (2008), shows that $P_1/2P_2$ does not exceed 0.53, which is far from the measured value which is 0.84. We conclude that the multiple periods of standing sausage modes measured so far remain to be explained.

Nevertheless, the sensitive dependence on the Alfvén Mach number of the cutoff aspect ratio $[(d/L)_{\rm cutoff}]$ has a number of observational implications. To show this, let us first examine this dependence further by conducting a parameter study for an extensive range of density contrast $[\rho_0/\rho_{\rm e}]$, the result of which is shown in Figure 11. Here the symbols represent $(d/L)_{\rm cutoff}$ as a function of M_A

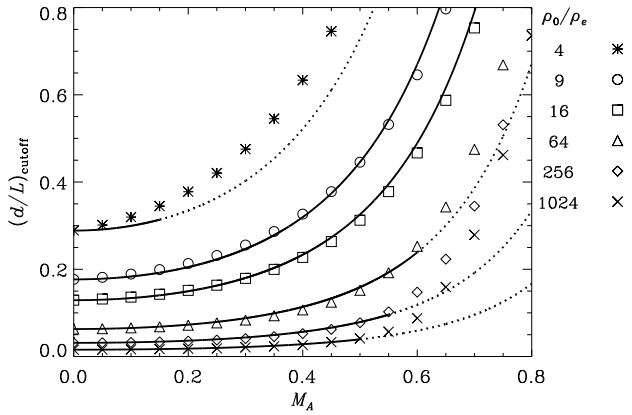

Figure 11. Aspect ratio cutoffs as functions of internal Alfvén Mach number $[M_A]$ for a series of density contrasts $[\rho_0/\rho_{\rm e}]$. In addition to the numerically derived values given by the symbols, an analytical fit $\left[1/\sqrt{4(\rho_0/\rho_{\rm e}-1)}\right]\exp\left(3.7M_A^2\right)$ is given by the curves. The curves are solid where this fit has an accuracy better than 10 %, and are dotted otherwise.

at a series of $\rho_0/\rho_{\rm e}$ ranging from 4 to 1024. The curves show an analytical fit

$$(d/L)_{\rm cutoff,fit} = \frac{1}{2}\sqrt{\frac{1}{\rho_0/\rho_{\rm e}-1}}\exp\left(3.7M_A^2\right). \tag{23}$$

The curves are solid where this fit is better than 10 % in accuracy and dotted otherwise. One sees that Equation (23) provides a good fit to the numerically derived $(d/L)_{\rm cutoff}$ for $\rho_0/\rho_{\rm e}$ ranging from 9 to 1024 and M_A in the range of $[0, 0.5]$.

The simplicity of Equation (23) makes it a convenient means to deduce the combination of $(\rho_0/\rho_{\rm e}, M_A)$ pertinent to a loop provided that it undergoes a standing sausage oscillation and that its aspect ratio is known. This is because, now that it does show oscillations in this particular mode, its aspect ratio has to be larger than determined by Equation (23). If the density contrast in this combination is further measured, then one readily derives an upper limit of M_A. Assuming $\rho_0/\rho_{\rm e} = 100$, if the loop aspect ratio is 0.12 (Nakariakov, Melnikov, and Reznikova, 2003), then one finds from Equation (23) that M_A has to be smaller than 0.49. If, on the other hand, taking d/L to be 0.03 (Srivastava *et al.*, 2008), one finds that if $\rho_0/\rho_{\rm e} = 600$, then M_A has to be smaller than 0.32. Given that measuring the flow magnitude in loops is a nontrivial task (Reale, 2010), this simple formula offers a tool for constraining the flow magnitude.

Actually, Equation (23) also enables one to take a further look at the standing sausage oscillations observed prior to the 2000s using radio bands with observing frequencies $\nu \lesssim 1$ GHz. This was done in Aschwanden, Nakariakov, and Melnikov (2004) (hereafter ANM04) who capitalized on the cutoff aspect ratios for static loops. At a given width-to-length ratio, taken to be 1/4 therein, for loops to support standing modes the density ratio has to exceed some critical value. However, the electron density of the loops n_0 as well as that of their surroundings

n_e are not arbitrary but observationally constrained. A natural constraint on n_0 comes from the observing frequency [ν] since the emission in this range comes primarily at the plasma frequency. As for n_e, a wealth of empirical data exists on which empirical formulae, such as the Baumbach–Allen one (Cox, 2000), were built. The point made by ANM04 is that, as n_e shows a height dependence, the ratio n_0/n_e (equivalent to ρ_0/ρ_e) may not exceed the critical value throughout the loop but only for a segment of it. While ANM04 adopt a formula valid for static loops, let us extend the idea therein to incorporate the flow effect as well. Figure 12 presents, similar to Figure 4 in ANM04, as functions of height h, the electron densities of the ambient corona [n_e] as well as the minimum loop density [n_0] required for loops with a width-to-length ratio [w/L] of 1/4 to support sausage modes. Here the Baumbach–Allen density is assumed for n_e, reading $n_e(h) \approx 4 \times 10^8/(1 + h/R_\odot)^9$ cm^{-3} with $R_\odot$ being the solar radius. On the other hand, n_0 is calculated for both the static case $M_A = 0$ and two flowing cases where $M_A = 0.2$ (the dotted curve) and 0.4 (dash–dotted), using the formula $n_0/n_e = 1 + \exp(7.4M_A^2)/(w/L)^2$. The latter formula simply follows from Equation (23). For comparison, the horizontal dashed line presents the density that corresponds to a plasma frequency of $\nu = 1$ GHz, calculated with the expression $(\nu/8980)^2$, in which ν is in Hz and the resulting density is in cm^{-3}. If an n_0 curve is below the dashed line, then the sausage mode is termed a "free" one by ANM04 in that the whole loop may experience the standing oscillations. However, if only part of an n_0 curve is below the dashed line, then only the loop segment that has heights above a certain value can experience sausage oscillations, which are termed "partial" modes by ANM04. As can be seen from Figure 12, while for $M_0 = 0$ this critical height reads 2.5 Mm, it increases substantially to 15 Mm when the loop flow corresponds to an M_A of 0.2, and further increases to 63.5 Mm when $M_A = 0.4$. From this we conclude that the flow effect should be taken into account when one tries to deduce the extent of the loop segment that can support a partial sausage mode.

4. Summary

The present study is motivated by the apparent lack of a detailed investigation into the effects of a significant field-aligned flow in coronal loops on standing modes that they support in general, the period ratios and cutoff aspect ratios in particular. By period ratios, we mean P_1/nP_n where P_1 stands for the period of the fundamental mode, and P_n represents the period of its $(n-1)^{\text{th}}$ overtone. The aspect ratio is defined as the ratio of loop half-width [d] to its length [L]. The Alfvén Mach number [M_A], which measures the loop flow speed in units of the internal Alfvén speed, is also relevant. Appropriate for coronal environments, the loops are modeled as a zero-β magnetic slab, where β is the ratio of the thermal to magnetic pressure. Our main results can be summarized as follows.

i) We presented a detailed analytical analysis of static slabs with transverse density structuring described by an Epstein profile. The results concern the behavior of P_1/nP_n in general, their behavior in the thin- and wide-slab limits in particular. By doing so, we generalize the study by Macnamara and Roberts

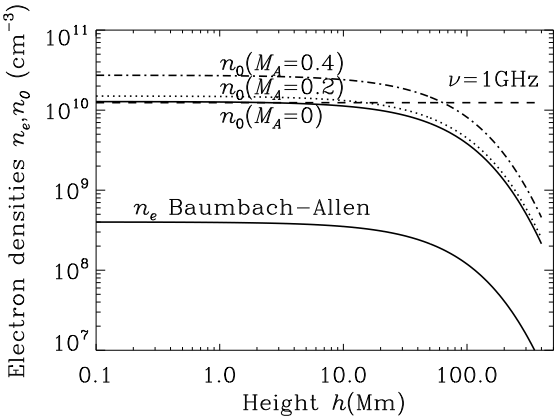

Figure 12. Height dependence of electron densities of loops [n_0] and their surroundings [n_e]. Here n_e is given by the Baumbach–Allen empirical model. Also given are a number of n_0, the minimum loop density for a loop with width-to-length ratio of 1/4 to support sausage modes. In addition to the static case, two flowing cases with internal Alfvén Mach numbers [M_A] being 0.2 (the dotted curve) and 0.4 (dash–dotted) are also given. For comparison, the density corresponding to a plasma frequency of 1 GHz is plotted by the dashed line.

(2011) to overtones of arbitrary order, and establish the lower bound that P_1/nP_n may attain. Solving the static-slab problem where the density profile is of a step-function form instead, we find that these lower limits also hold.

ii) For standing kink modes supported by flowing slabs, the flow is found to significantly reduce the period ratios [P_1/nP_n] for all of the considered density contrasts [ρ_0/ρ_e]. This is true even when ρ_0/ρ_e is very large (the solid curves in Figure 7), in which case while for static slabs P_1/nP_n almost reaches the analytically expected lower limit [$1/\sqrt{n}$], they may be reduced by [13.7 %, 20.3 %, 24.5 %] for n being [2, 3, 4] for the Alfvén Mach number [M_A] in the range of [0, 0.8]. For lower, and therefore more realistic, density contrasts, the flow effect is even stronger.

iii) A way of deducing simultaneously ρ_0/ρ_e and M_A, pertinent to standing kink modes, is illustrated in Figure 8. The idea is simply that, if the main contributor to the departure of P_1/nP_n from unity is the wave dispersion due to transverse structuring in density and flow speeds, then at a given aspect ratio, if P_1/nP_n with two different n are measured, the combination of $(\rho_0/\rho_e, M_A)$ may be readily read out from a contour plot similar to Figure 8. In fact, if an additional overtone is also measured, an uncertainty measure of the deduced $(\rho_0/\rho_e, M_A)$ can be readily deduced.

iv) For standing sausage modes supported by flowing slabs, the flow effect on P_1/nP_n is not as strong but still substantial in reducing their values at a given slab aspect ratio. However, in the flowing case P_1/nP_n is still bounded by the lower limit $1/n$ established for static slabs, the reason being that the flow significantly enhances the cutoff aspect ratio, below which sausage modes are no longer trapped.

v) A parameter study on the cutoff aspect ratio for standing sausage modes [$(d/L)_{\rm cutoff}$] yields that it may be satisfactorily approximated by Equation (23).

which involves ρ_0/ρ_e and M_A in a simple manner, when ρ_0/ρ_e is in the range of $[9, 1024]$ and M_A in the range $[0, 0.5]$. This simple formula allows one to analytically constrain ρ_0/ρ_e and M_A making use of only the fact that a loop experiences standing sausage oscillations. Provided that the aspect ratio is known, if the density contrast is found as well, then one readily derives the upper limit for M_A.

vi) The simple formula of Equation (23) enables us to deduce that, if the Baumbach–Allen model can describe the density of the ambient corona, and if the loops in radio observations with observing frequencies lower than 1 GHz as compiled by Aschwanden, Nakariakov, and Melnikov (2004) correspond to a width-to-length ratio of 1/4, then only the segment at heights above 15 (64) Mm can experience a partial sausage oscillation when M_A is 0.2 (0.4), which are substantially higher than 2.5 Mm found in the static case. This expands the original discussion on sausage modes confined to only a loop segment rather than perturbing the entire loop (Aschwanden, Nakariakov, and Melnikov, 2004).

Acknowledgements This research is supported by the 973 program 2012CB825601, the National Natural Science Foundation of China (40904047, 41174154, and 41274176), the Ministry of Education of China (20110131110058 and NCET-11-0305), and by the Provincial Natural Science Foundation of Shandong via Grant JQ201212.

References

Andries, J., van Doorsselaere, T., Roberts, B., Verth, G., Verwichte, E., Erdélyi, R.: 2009, *Space Sci. Rev.* **149**, 3.
Andries, J., Arregui, I., Goossens, M.: 2005, *Astrophys. J. Lett.* **624**, L57.
Aschwanden, M.J., Schrijver, C.J.: 2011, *Astrophys. J.* **736**, 102.
Aschwanden, M.J., Nakariakov, V.M., Melnikov, V.F.: 2004, *Astrophys. J.* **600**, 458.
Aschwanden, M.J., Fletcher, L., Schrijver, C.J., Alexander, D.: 1999, *Astrophys. J.* **520**, 880.
Banerjee, D., Erdélyi, R., Oliver, R., O'Shea, E.: 2007, *Solar Phys.* **246**, 3. ADS:2007SoPh..246....3B, doi:10.1007/s11207-007-9029-z.
Cooper, F.C., Nakariakov, V.M., Williams, D.R.: 2003, *Astron. Astrophys.* **409**, 325.
Cox, A.N.:2000, *Allen's Astrophysical Quantities*, AIP.
De Moortel, I.: 2009, *Space Sci. Rev.* **149**, 65.
De Moortel, I.: 2006, *Roy Soc London Phil. Trans. Series A* **364**, 461.
De Moortel, I., Brady, C.S.: 2007, *Astrophys. J.* **664**, 1210.
De Moortel, I., Nakariakov, V.M.: 2012, *Roy Soc London Phil Trans Series A* **370**, 3193.
Donnelly, G.R., Díaz, A.J., Roberts, B.: 2006, *Astron. Astrophys.* **457**, 707.
Edwin, P.M., Roberts, B.: 1982, *Solar Phys.* **76**, 239. ADS:1982SoPh...76..239E, doi:10.1007/BF00170986.
Edwin, P.M., Roberts, B.: 1988, *Astron. Astrophys.* **192**, 343.
Erdélyi, R., Goossens, M.: 2011, *Space Sci. Rev.* **158**, 167.
Erdélyi, R., Taroyan, Y.: 2008, *Astron. Astrophys.* **489**, L49.
Erdélyi, R., Hague, A., Nelson, C.J.: 2013, *Solar Phys.*, 195. doi:10.1007/s11207-013-0344-2.
Handy, B.N., Acton, L.W., Kankelborg, C.C., Wolfson, C.J., Akin, D.J., Bruner, M.E., Caravalho, R., Catura, R.C., Chevalier, R., Duncan, D.W., Edwards, C.G., Feinstein, C.N., Freeland, S.L., Friedlaender, F.M., Hoffmann, C.H., Hurlburt, N.E., Jurcevich, B.K., Katz, N.L., Kelly, G.A., Lemen, J.R., Levay, M., Lindgren, R.W., Mathur, D.P., Meyer, S.B., Morrison, S.J., Morrison, M.D., Nightingale, R.W., Pope, T.P., Rehse, R.A., Schrijver, C.J., Shine, R.A., Shing, L., Strong, K.T., Tarbell, T.D., Title, A.M., Torgerson, D.D., Golub, L., Bookbinder, J.A., Caldwell, D., Cheimets, P.N., Davis, W.N., Deluca, E.E., McMullen, R.A., Warren, H.P., Amato, D., Fisher, R., Maldonado, H., Parkinson, C.: 1999, *Solar Phys.* **187**, 229. ADS:1999SoPh..187..229H, doi:10.1023/A:1005166902804.

Harra, L.K., Démoulin, P., Mandrini, C.H., Matthews, S.A., van Driel-Gesztelyi, L., Culhane, J.L., Fletcher, L.: 2005, *Astron. Astrophys.* **438**, 1099.

Howard, R.A., Moses, J.D., Vourlidas, A., Newmark, J.S., Socker, D.G., Plunkett, S.P., Korendyke, C.M., Cook, J.W., Hurley, A., Davila, J.M., Thompson, W.T., St Cyr, O.C., Mentzell, E., Mehalick, K., Lemen, J.R., Wülser, J.P., Duncan, D.W., Tarbell, T.D., Wolfson, C.J., Moore, A., Harrison, R.A., Waltham, N.R., Lang, J., Davis, C.J., Eyles, C.J., Mapson-Menard, H., Simnett, G.M., Halain, J.P., Defise, J.M., Mazy, E., Rochus, P., Mercier, R., Ravet, M.F., Delmotte, F., Auchère, F., Delaboudinière, J.P., Bothmer, V., Deutsch, W., Wang, D., Rich, N., Cooper, S., Stephens, V., Maahs, G., Baugh, R., McMullin, D., Carter, T.: 2008, *Space Sci. Rev.* **136**, 67.

Inglis, A.R., van Doorsselaere, T., Brady, C.S., Nakariakov, V.M.: 2009, *Astron. Astrophys.* **503**, 569.

Innes, D.E., McKenzie, D.E., Wang, T.: 2003, *Solar Phys.* **217**, 267. ADS:2003SoPh..217..267I, doi:10.1023/B:SOLA-0000006874-31799-bc.

Kaiser, M.L., Kucera, T.A., Davila, J.M., St. Cyr, O.C., Guhathakurta, M., Christian, E.: 2008, *Space Sci. Rev.* **136**, 5.

Kosugi, T., Matsuzaki, K., Sakao, T., Shimizu, T., Sone, Y., Tachikawa, S., Hashimoto, T., Minesugi, K., Ohnishi, A., Yamada, T., Tsuneta, S., Hara, H., Ichimoto, K., Suematsu, Y., Shimojo, M., Watanabe, T., Shimada, S., Davis, J.M., Hill, L.D., Owens, J.K., Title, A.M., Culhane, J.L., Harra, L.K., Doschek, G.A., Golub, L.: 2007, *Solar Phys.* **243**, 3. ADS:2007SoPh..243....3K, doi:10.1007/s11207-007-9014-6.

Kupriyanova, E.G., Melnikov, V.F., Shibasaki, K.: 2013, *Solar Phys.* **284**, 559. ADS:10.1007/s11207-012-0141-3, doi:2013SoPh..284..559K

Landau, L., Lifshitz, E.: 1958, *Quantum Mechanics*, Pergamon Press.

Lemen, J.R., Title, A.M., Akin, D.J., Boerner, P.F., Chou, C., Drake, J.F., Duncan, D.W., Edwards, C.G., Friedlaender, F.M., Heyman, G.F., Hurlburt, N.E., Katz, N.L., Kushner, G.D., Levay, M., Lindgren, R.W., Mathur, D.P., McFeaters, E.L., Mitchell, S., Rehse, R.A., Schrijver, C.J., Springer, L.A., Stern, R.A., Tarbell, T.D., Wuelser, J.-P., Wolfson, C.J., Yanari, C., Bookbinder, J.A., Cheimets, P.N., Caldwell, D., Deluca, E.E., Gates, R., Golub, L., Park, S., Podgorski, W.A., Bush, R.I., Scherrer, P.H., Gummin, M.A., Smith, P., Auker, G., Jerram, P., Pool, P., Soufli, R., Windt, D.L., Beardsley, S., Clapp, M., Lang, J., Waltham, N.: 2012, *Solar Phys.* **275**, 17. ADS:2012SoPh..275...17L, doi:10.1007/s11207-011-9776-8.

Li, B., Habbal, S.R., Chen, Y.: 2013, *Astrophys. J.* **767**, 169.

Liu, W., Title, A.M., Zhao, J., Ofman, L., Schrijver, C.J., Aschwanden, M.J., De Pontieu, B., Tarbell, T.D.: 2011, *Astrophys. J. Lett.* **736**, L13.

Macnamara, C.K., Roberts, B.: 2011, *Astron. Astrophys.* **526**, A75.

McEwan, M.P., Donnelly, G.R., Díaz, A.J., Roberts, B.: 2006, *Astron. Astrophys.* **460**, 893.

Melnikov, V.F., Reznikova, V.E., Shibasaki, K., Nakariakov, V.M.: 2005, *Astron. Astrophys.* **439**, 727.

Nakariakov, V.M., Erdélyi, R.: 2009, *Space Sci. Rev.* **149**, 1.

Nakariakov, V.M., Roberts, B.: 1995a, *Solar Phys.* **159**, 213. ADS:1995SoPh..159..213N, doi:10.1007/BF00686530.

Nakariakov, V.M., Roberts, B.: 1995b, *Solar Phys.* **159**, 399. ADS:1995SoPh..159..399N, doi:10.1007/BF00686541.

Nakariakov, V.M., Hornsey, C., Melnikov, V.F.: 2012, *Astrophys. J.* **761**, 134.

Nakariakov, V.M., Melnikov, V.F., Reznikova, V.E.: 2003, *Astron. Astrophys.* **412**, L7.

Nakariakov, V.M., Verwichte, E.: 2005, *Liv. Rev. Solar Phys.* **2**, 3. doi:10.12942/lrsp-2005-3.

Nakariakov, V.M., Ofman, L., Deluca, E.E., Roberts, B., Davila, J.M.: 1999, *Science* **285**, 862.

Ofman, L., Aschwanden, M.J.: 2002, *Astrophys. J.* **576**, L153.

Ofman, L., Wang, T.J.: 2008, *Astron. Astrophys.* **482**, L9.

Pascoe, D.J., Nakariakov, V.M., Arber, T.D.: 2007, *Astron. Astrophys.* **461**, 1149.

Pesnell, W.D., Thompson, B.J., Chamberlin, P.C.: 2012, *Solar Phys.* **275**, 3. ADS:2012SoPh..275....3P, doi:10.1007/s11207-011-9841-3.

Reale, F.: 2010, *Liv. Rev. Solar Phys.* **7**, 5. doi:10.12942/lrsp-2010-5.

Roberts, B.: 2000, *Solar Phys.* **193**, 139. ADS:2000SoPh..193..139R, doi:10.1023/A:1005237109398.

Roberts, B.: 2008, In: Erdélyi, R., Mendoza-Briceño, C.A. (eds.), *Waves & Oscillations in the Solar Atmosphere: Heating and Magneto-Seismology*, *IAU Symp.* **247**, Cambridge Univ. Press, 3.

Ruderman, M.S.: 2010, *Solar Phys.* **267**, 377. ADS:2010SoPh..267..377R, doi:10.1007/s11207-010-9668-3.

Ruderman, M.S., Erdélyi, R.: 2009, *Space Sci. Rev.* **149**, 199.
Ruderman, M.S., Verth, G., Erdélyi, R.: 2008, *Astrophys. J.* **686**, 694.
Srivastava, A.K., Zaqarashvili, T.V., Uddin, W., Dwivedi, B.N., Kumar, P.: 2008, *Mon. Not. Roy. Astron. Soc.* **388**, 1899.
Terradas, J., Arregui, I., Verth, G., Goossens, M.: 2011, *Astrophys. J. Lett.* **729**, L22.
Van Doorsselaere, T., Birtill, D.C.C., Evans, G.R.: 2009, *Astron. Astrophys.* **508**, 1485.
Van Doorsselaere, T., Nakariakov, V.M., Verwichte, E.: 2007, *Astron. Astrophys.* **473**, 959.
Verth, G., Erdélyi, R.: 2008, *Astron. Astrophys.* **486**, 1015.
Verwichte, E., Foullon, C., Van Doorsselaere, T.: 2010, *Astrophys. J.* **717**, 458.
Verwichte, E., Nakariakov, V.M., Cooper, F.C.: 2005, *Astron. Astrophys.* **430**, L65.
Verwichte, E., Nakariakov, V.M., Ofman, L., Deluca, E.E.: 2004, *Solar Phys.* **223**, 77. ADS:2004SoPh..223...77V, doi:10.1007/s11207-004-0807-6.
Verwichte, E., Aschwanden, M.J., Van Doorsselaere, T., Foullon, C., Nakariakov, V.M.: 2009, *Astrophys. J.* **698**, 397.
Wang, T.: 2011, *Space Sci. Rev.* **158**, 397.
White, R.S., Verwichte, E.: 2012, *Astron. Astrophys.* **537**, A49.
Williams, D.R., Phillips, K.J.H., Rudawy, P., Mathioudakis, M., Gallagher, P.T., O'Shea, E., Keenan, F.P., Read, P., Rompolt, B.: 2001, *Mon. Not. Roy. Astron. Soc.* **326**, 428.
Williams, D.R.,Mathioudakis, M., Gallagher, P.T., Phillips, K.J.H., McAteer, R.T.J., Keenan, F.P., Rudawy, P., Katsiyannis, A.C.: 2002, *Mon. Not. Roy. Astron. Soc.* **336**, 747.